BEILSTEIN ARCHIVES

This open access document is posted as a preprint in the Beilstein Archives at https://doi.org/10.3762/bxiv.2020.140.v1 and is considered to be an early communication for feedback before peer review. Before citing this document, please check if a final, peer-reviewed version has been published.

This document is not formatted, has not undergone copyediting or typesetting, and may contain errors, unsubstantiated scientific claims or preliminary data.

Preprint Title High-throughput free surface electrospinning using solution reservoirs with different depths and its preparation mechanism study

Authors Jing Yin, Adnan Ahmed and Lan Xu

Publication Date 10 Dez. 2020

Article Type Full Research Paper

ORCID® iDs Jing Yin - https://orcid.org/0000-0002-4645-9517; Adnan Ahmed - https://orcid.org/0000-0002-5095-7463; Lan Xu - https://orcid.org/0000-0003-2185-4104

License and Terms: This document is copyright 2020 the Author(s); licensee Beilstein-Institut.

This is an open access work under the terms of the Creative Commons Attribution License (https://creativecommons.org/licenses/by/4.0). Please note that the reuse, redistribution and reproduction in particular requires that the author(s) and source are credited and that individual graphics may be subject to special legal provisions.
The license is subject to the Beilstein Archives terms and conditions: https://www.beilstein-archives.org/xiv/terms.
The definitive version of this work can be found at https://doi.org/10.3762/bxiv.2020.140.v1

High-throughput free surface electrospinning using solution reservoirs with different depths and its preparation mechanism study

Jing Yin, Adnan Ahmed, Lan Xu*

National Engineering Laboratory for Modern Silk, College of Textile and Engineering, Soochow University, 199 Ren-ai Road, Suzhou 215123, China
*Corresponding author.
E-mails: 20184215040@stu.suda.edu.cn (J. Yin), adnanahmed0070@outlook.com (A. Ahmed), lanxu@suda.edu.cn (L. Xu).

[1] Jing Yin and Adnan Ahmed contributed equally to this paper.

Abstract

This paper presented a self-made spherical section free surface electrospinning (SSFSE) using solution reservoirs with different depths for obtaining high-throughput production of nanofibers, and studied its preparation mechanism. The effects of the solution reservoir depth on the SSFSE process as well as the quality and yield of polyacrylonitrile (PAN) nanofibers were investigated experimentally using high-speed camera, precise electronic balance and scanning electron microscopy, and were analyzed theoretically by response surface methodology (RSM) and numerical simulation. The values predicted by the established RSM model and the electric field simulation results obtained by Maxwell 3D were all consistent with the experimental data, which showed that the solution reservoir depth had little effects on the quality of PAN nanofibers, but had great effects on the yields of them. When the maximum depth of solution reservoir was 4.29 mm, the PAN nanofibers prepared have the best quality and the highest yields.

Keywords: Free surface electrospinning; Nanofibers; High-throughput production; Response surface methodology; Electric field simulation

1. Introduction

Due to their characteristics of high specific surface area and aspect ratio, nanofibers are widely used in tissue engineering [1, 2], filtration [3], wound dressings [4], sound-absorbing materials [5], food preservation [6] and so on. At present, the technologies for preparing nanofibers have self-assembly [7], phase separation [2], electrospinning (ES) [8-11], and so on. ES is one of the easiest ways to prepare nanofibers continuously. With the increasing demand for nanofibers, more and more attention has been paid to the high-throughput production of nanofibers. However, the yield of traditional single-needle ES (0.01-1g/h) is too low, which limits its commercial application [12-14]. Multi-needle ES is considered as an effective method to increase the yield of nanofibers, but it has some disadvantages, such as complicated design and potential clogging [14, 15]. Therefore, needleless ES (NES) is presented to overcome the disadvantages of multi-needle electrospinning and realize the high-throughput preparation of nanofibers [16]. NES usually means that the free surface of the spinning solution is subjected to

fluctuations under the action of a high electric field, overcoming the surface tension of the solution, forming many jets and then stretching into nanofibers [17]. In recent years many types of needleless ES have been proposed for mass production of nanofibers, such as rotating shaft ES [18], free surface electrospinning (FSE) [19], bubble ES (BE) [20], and so on [21].

In our previous researches [4, 22-26], a series of self-made NES devices for mass production of nanofibers have been developed and applied, such as modified MBE [22-24], sloping FSE (SFSE) [4], oblique section FSE (OSFSE) [25], spherical section FSE (SSFSE) [26]. According to these researches it was found that SSFSE was the optimal NES device for preparing nanofibers with the highest quality and yield. On this basis, the SSFSE with a replaceable solution reservoir was designed to obtain high-throughput production of nanofibers, as shown in Fig.1, and the influence of the solution reservoir radius on the spinning effects of SSFSE was studied, which indicated the SSFSE device using the solution reservoir with a radius of 25mm could provide the highest quality and yield of nanofibers [26].

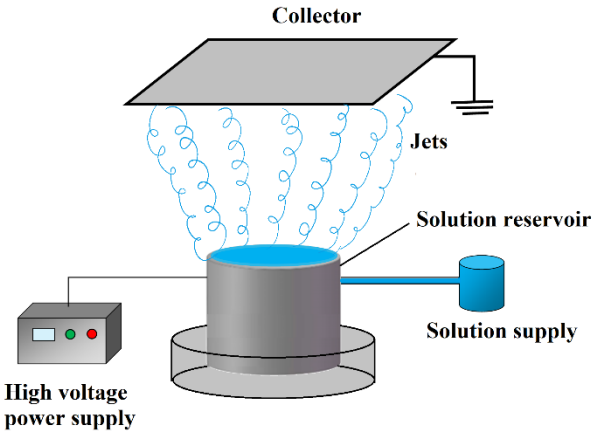

Figure 1: Schematic of the SSFSE device with a replaceable solution reservoir

In this paper, the influences of the solution reservoir depth on the spinning effects of SSFSE were investigated experimentally by a combination of high-speed camera, precise electronic balance and scanning electron microscopy. Response surface methodology (RSM) involving central composite design (CCD) was applied to model and optimize the SSFSE process for evaluating the influence of spinning parameters on the yield of polyacrylonitrile (PAN) nanofibers. And the preparation mechanism of the SSFSE device was studied by simulating the electric field distribution in the spinning process using Maxwell 3D. The RSM predicted values and the electric field simulation results were all consistent with the experimental data, which showed that the SSFSE device with different solution reservoir could produce nanofibers with higher quality and yield, and the solution reservoir depth had great effects on the yields of them. When the maximum depth of solution reservoir was 4.29 mm, the highest quality and yield of PAN nanofibers were fabricated.

2. Materials and methods

2.1. Materials

Polyacrylonitrile (PAN, Mw = 15w) was obtained from Beijing Lark Branch Co., Ltd. (Beijing, China). Sodium dodecylbenzene sulfonate (SDBS) was purchased from Sinopharm Chemical Reagent Co. Ltd. (Shanghai, China). N, N-dimethylformamide (DMF) was supplied from Shanghai Chemical Reagent Co., Ltd. (Shanghai, China). For obtaining the spinning solutions, 10% PAN and 1% SDBS were dissolved in DMF under magnetic stirring at 60°C for 4h to get transparent liquid using a thermostatic magnetic stirrer (DF-101S, Xinrui Instrument Factory, Changzhou, China).

2.2. Apparatus

The replaceable solution reservoir of the SSFSE is made of a copper cylinder with a height of 40mm and a diameter of 50mm. There are five solution reservoirs with different maximum depths, which are obtained by truncating the copper cylinder using spheres with a radius of 45 mm, 55 mm, 65 mm, 75 mm and 85 mm respectively, as illustrated in Fig. 2. And the maximum depths (h), the areas of spherical section (S) and the solution storage volumes (V) of the five solution reservoirs are calculated according to the different sphere radii (R), as shown in Table 1.

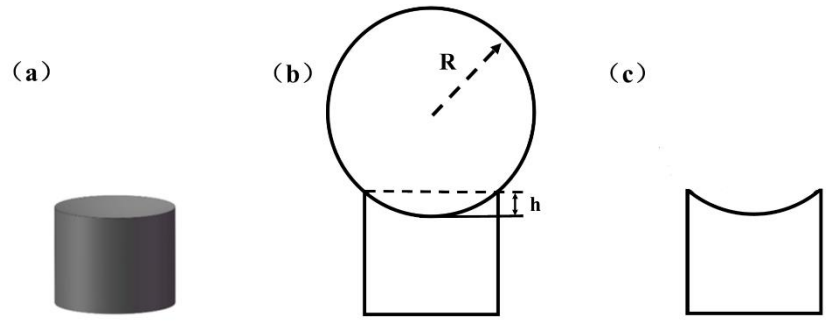

Figure 2: Schematic diagram of the SSFSE solution reservoir truncated by a sphere. (a) is the 3D schematic diagram. (b) indicates the sphere which truncate the solution reservoir. (c) is the longitudinal cross-section view

Table 1 The maximum depth (h), the area of spherical section (S), the solution storage volume(V) of the solution reservoir obtained by different sphere radii

R(mm)	h (mm)	S (mm^2)	V (mm^3)
45	7.58	2143.08	7673.36
55	6.01	2075.92	6010.73
65	5	2041	4974.19
75	4.29	2020.27	4250.08
85	3.76	2006.88	3718.82

2.3. Self-made SSFSE processes

According to the reference [26], the SSFSE parameters were set as follows: the room temperature was 20℃, the relative humidity was 70%, the receiving area was 200 mm × 200 mm, the receiving distance was 180 mm, and the applied voltages were 35 kV, 40 kV and 45 kV. The spinning processes of the SSFSE solution reservoirs with different depths were investigated by a high-speed camera (VRI Phantom-VEO-L, Ametek, California, USA), and the initial voltages of them were determined

respectively, as shown in Fig.3. It could be seen that as the solution reservoir depth increased the initial voltage increased, due to the point discharge at the top edge of the reservoirs. And with the increase of the applied voltage, the number of jets on the solution surface increased gradually. However, when the applied voltage was too high (45 kV), the jets became unstable and uneven. In addition, the decrease of the solution reservoir depth also enhanced the number of jets on the solution surface because of the higher electric field intensity and more uniform electric field distribution. The experiment results would be verified by simulating the electric field distribution in the SSFSE processes.

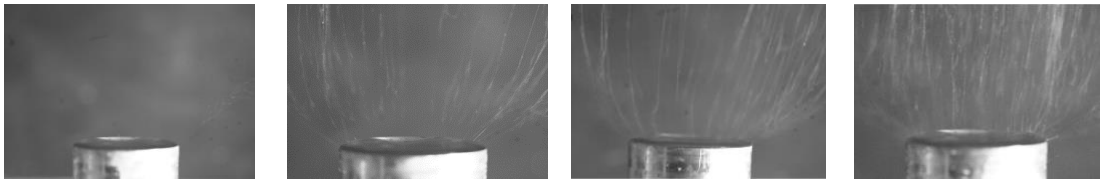

Initial voltage 25kV 35kV 40kV 45kV

(a) SSFSE solution reservoir with a maximum depth of 7.58 mm

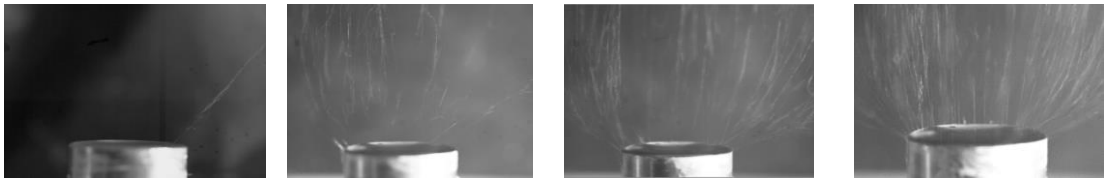

Initial voltage 26kV 35kV 40kV 45kV

(b) SSFSE solution reservoir with a maximum depth of 6.01 mm

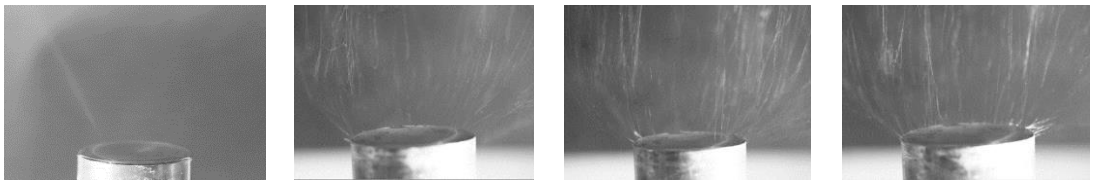

Initial voltage 28kV 35kV 40kV 45kV

(c) SSFSE solution reservoir with a maximum depth of 5 mm

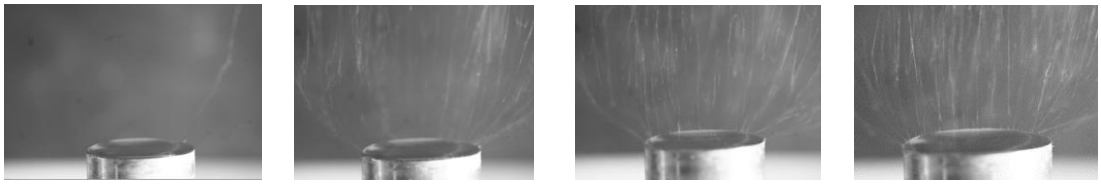

Initial voltage 30kV 35kV 40kV 45kV

(d) SSFSE solution reservoir with a maximum depth of 4.29 mm

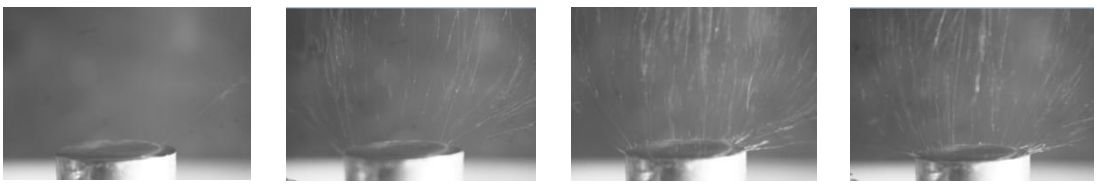

Initial voltage 32kV 35kV 40kV 45kV

(e) SSFSE solution reservoir with a maximum depth of 3.76 mm

Figure 3: Pictures of SSFSE processes of the solution reservoirs with different depths at different voltages

2.4. Characterization

2.4.1. Yield of nanofibers

The masses of PAN nanofibers prepared after spinning for 30 min were measured by a precise electronic balance (XJ120A, Precisa, Shanghai, China), and each of the measurements was repeated five times to obtain the average value. Due to the same area of spinning surface, the calculation method of yield is as follows:

$$W = (W_1 - W_0)/t \quad (1)$$

where W is the yield of nanofibers, W_0 and W_1 are the masses of the aluminum foils before and after spinning respectively, and t is the spinning time.

2.4.2. Morphology of nanofibers

The scanning electron microscopy (SEM, Hitachi S4800, Hitachi, Tokyo, Japan) was used to investigate the morphology of PAN nanofibers. And 10 SEM pictures and 100 nanofibers at random in each SEM picture of every sample were used to analyze the diameter distribution of nanofibers by Image J software (National Institute of Mental Health, Bethesda, MD, USA).

2.4.3. Response surface method and design of experiments

The response surface method (RSM) can be applied to optimize and design experiments, which has the advantages of fewer experiments, higher accuracy and better predictable performance. Central composite design (CCD) as a standard RSM design can be used for modeling, analysis and optimization of electrospinning[26]. Because the solution reservoir depth was determined by the radius of a sphere that truncated the reservoir, two factors were two SSFSE parameters: the sphere radius and applied voltage, and the response was the yield of PAN nanofibers. The two factors and factor levels were exhibited in Table 2. Based on CCD, an approximate mathematical relationship between the response and the two factors (A: Sphere radius and B: voltage) could be established by the following quadratic polynomial model [27, 28]:

$$\mathrm{Y} = \beta_0 + \beta_1 \mathrm{A} + \beta_2 \mathrm{B} + \beta_3 \mathrm{A}^2 + \beta_4 \mathrm{B}^2 + \beta_5 \mathrm{AB} \quad (2)$$

where Y is the value of the yield of nanofibers, A is the value of the sphere radius, B is the value of the applied voltage, β_0, β_1, β_2, β_3, β_4 and β_5 are undetermined coefficients which can be estimated by experimental data.

The probability value (P-value) is presented to investigate the statistical significance of factors. P-values lower than 0.05 are considered as statistically meaningful values, which illustrate the factors have significant effects on the response [29]. R-squared (R^2) is an important indicator to indicate the statistical significance of the model, which determines how well the model agrees with the experimental results.

Table 2 The factors and factor levels for experimental design

Factors	Factors levels
A: Sphere radius (mm)	45, 55, 65, 75, 85
B: Applied voltage (kV)	35, 40, 45

2.4.4. Simulation of the electric field

The electric field distributions from the solution reservoir to the collector in the SSFSE processes with solution reservoirs of different depths were simulated using Maxwell 3D. The electric field simulations for these SSFSE processes were performed by the following experimental parameters: the copper reservoirs as positive poles were cylinders with a diameter of 50 mm and a height of 40 mm, which were truncated by spheres with a radius of 45mm, 55mm, 65mm, 75mm and 85mm, respectively, the

electric conductivity of copper was 5.8 × 10^{11} μs/cm, the electric conductivity of PAN solution was 2372 μs/cm, the applied voltage was 40 kV, and the distance from the solution surface to the collector was 180 mm.

3. Result and discussion

3.1. Yield of PAN nanofibers

Fig.4 illustrated the yields of PAN nanofibers fabricated by the different SSFSE devices at the different applied voltage. It could be found that with the increase of the voltage the yield of PAN nanofibers obtained by the same SSFSE device increased, and with the decrease of the solution reservoir depth the yield of nanofibers first increased and then decreased at the same voltage. When the maximum depth of the solution reservoir was 3.76 mm at the applied voltages of 40 kV and 45 kV, the yields of nanofibers were all lower than those when the maximum depth of the solution reservoir was 4.29 mm. This was because lots of jets were unstable and spread outward due to too high electric field intensity, as indicated in Fig.3 (e). These outward expanding jets and too high spinning speed made it difficult for nanofibers to be collected on the collector, leading to the decrease of the yield of nanofibers. When the applied voltage was 45 kV and the maximum depth of the solution reservoir was 4.29 mm, the yield of nanofibers reached a maximum of 27.34 g/h. The experiment results agreed with the observed phenomena by a high-speed camera, which would be confirmed by RSM and electric field simulation analysis. In addition, it was noticed that when the maximum depths of the solution reservoirs were 5 mm, 4.29 mm and 3.76 mm, the yields of nanofibers prepared at 40 kV were similar to those at 45 kV. Considering the stability of the spinning process, the effect of the solution reservoir depth on the morphology of PAN nanofibers prepared at 40 kV would be investigated.

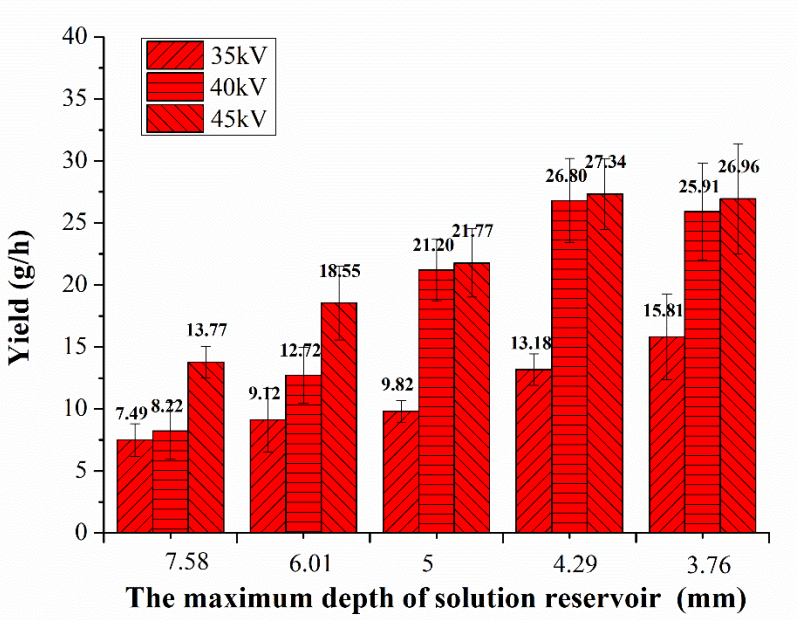

Figure 4: Yield of PAN nanofibers prepared by different SSFSE solution reservoirs at different voltages

3.2. Morphology of nanofibers

Fig.5 showed the morphology of PAN nanofibers prepared by five SSFSE solution reservoirs with different depths at the voltage of 40 kV and the corresponding nanofiber diameter distributions. Meanwhile, the average diameters and confidence intervals of these nanofibers were indicated in Fig.5 (a-2,b-2,c-2,d-2,e-2). It could be seen that these PAN nanofibers were of good quality due to the good spinning effects of these SSFSE

processes with five solution reservoirs of different depths. But as the solution reservoir depth decreased, the average diameter of the prepared PAN nanofibers first increased and then decreased, and the uniformity of their diameter distributions all increased. When the maximum depth of the solution reservoir was 7.58 mm, the average diameter of the prepared nanofibers was smaller, but its diameter distributions was the most nonuniform due to the tip discharge generated by the sharpest top edge of the reservoir. When the maximum depth of the solution reservoir was 3.76 mm, the average diameter of nanofibers was the largest and its diameter distribution was most uniform because too fast spinning speed made the jet not fully stretched due to the smallest reservoir depth and the weakening of the tip discharge phenomenon. When the maximum depth of the solution reservoir was 4.29 mm, the average diameter of nanofibers was minimum and its diameter distribution was more uniform.

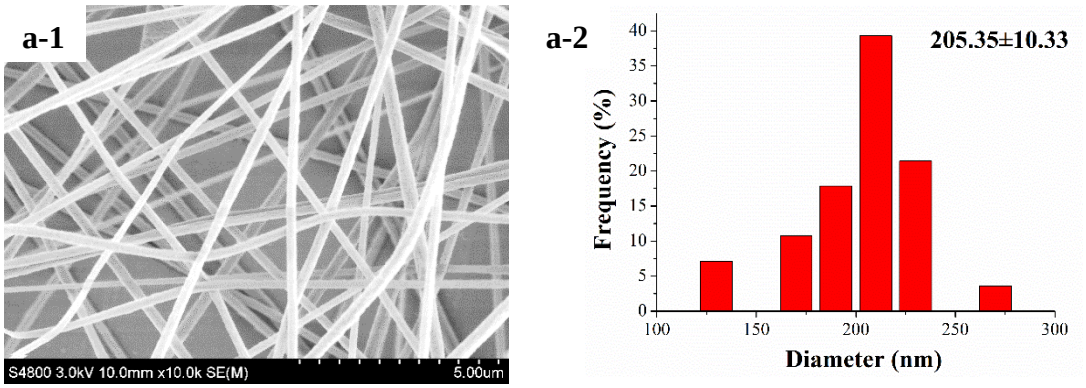

(a) SSFSE solution reservoir with a maximum depth of 7.58 mm

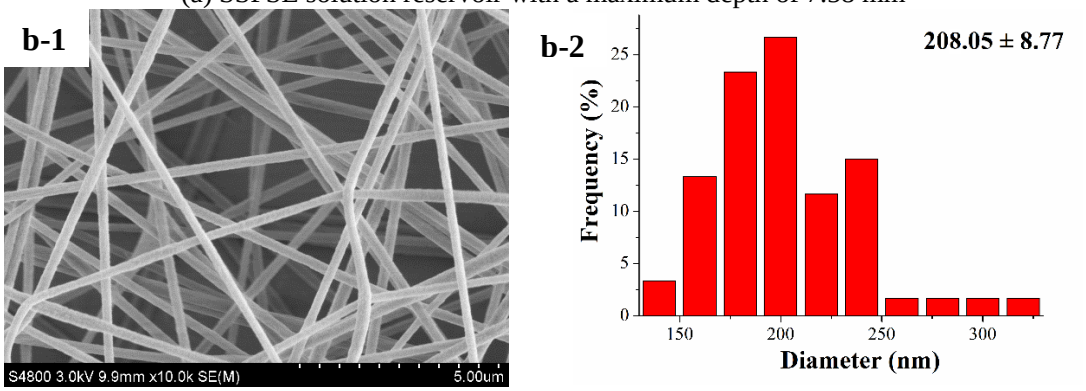

(b) SSFSE solution reservoir with a maximum depth of 6.01 mm

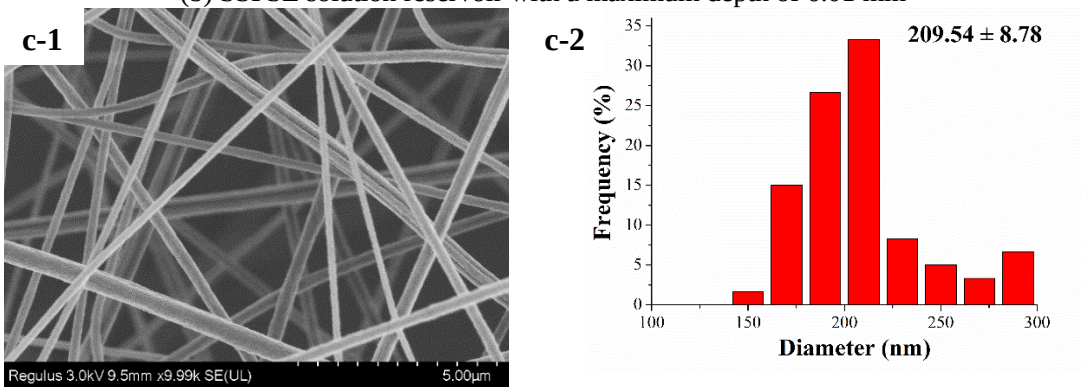

(c) SSFSE solution reservoir with a maximum depth of 5 mm

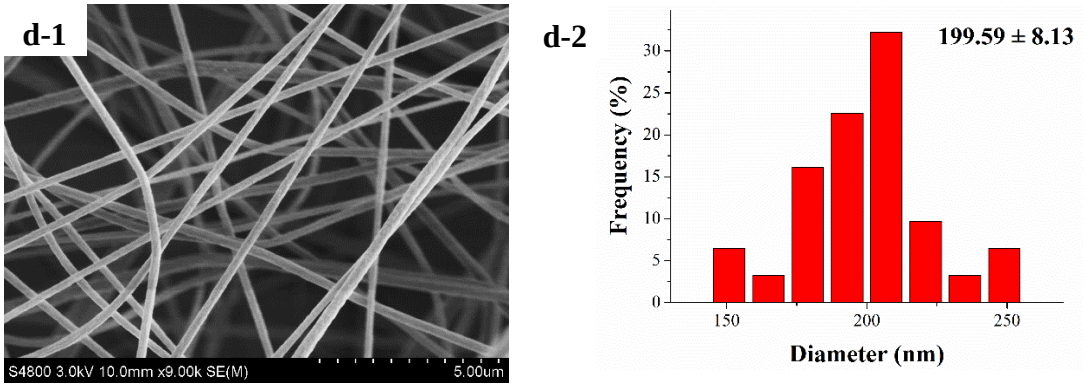

(d) SSFSE solution reservoir with a maximum depth of 4.29 mm

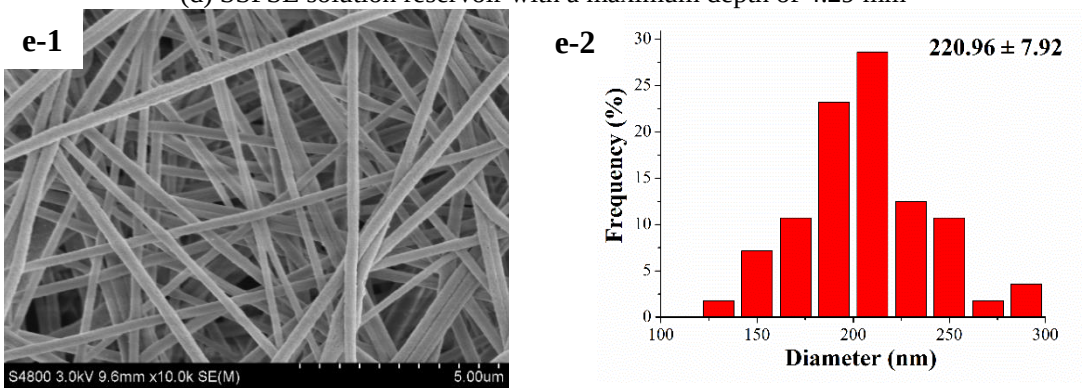

(e) SSFSE solution reservoir with a maximum depth of 3.76 mm

Figure 5: SEM pictures and the corresponding diameter distributions of PAN nanofiber prepared by the SSFSE solutions reservoirs with different depths

3.3. Response function

The effects of different sphere radius (A) and applied voltage (B) on the yield of PAN nanofibers were studied using the CCD technique. The 15 groups of experiments designed by the CCD method were shown in Table 3.

Table 3 Experimental design and response.

Run	Factors (actual values)		Response (actual values)
	A: Sphere radius (mm)	B: Voltage (kV)	Yield (g/h)
1	45	35	7.494
2	45	40	8.225
3	45	45	13.77
4	55	35	9.12
5	55	40	12.72
6	55	45	18.55
7	65	35	9.82
8	65	40	21.205
9	65	45	21.765
10	75	35	13.1775
11	75	40	26.80
12	75	45	27.34
13	85	35	15.808
14	85	40	25.91
15	85	45	26.96

To obtain a quadratic polynomial equation and statistical analysis of the acquired data, the analysis of variance (ANOVA) was performed according to Eq. (2), and P-

values and R^2 were determined [28], which were listed in Table 4. It indicated P-values for the model and terms (A and B) were less than 0.05, which demonstrated the model and the two terms had significant influence on the response (the yield of nanofibers). R^2 was 0.9208, which showed that the predicted value of the model agreed with the actual value. Therefore, the quadratic response surface model for the yield of nanofibers could be expressed as the following equation:

$$Y = 19.78 + 7.02A + 5.30B + 1.45A^2 - 1.61B^2 - 2.59AB \quad (3)$$

According to Eq. (3), the predicted yields of nanofibers were plotted, as shown in Fig. 6. The actual values of yields of nanofibers were distributed along the predicted curve, which indicated the predicted values were in agreement with the experimental data, illustrating that the model was suitable for the experimental data.

Table 4 ANOVA for the quadratic regression model.

Source	Sum of squares	Degree of freedom	Mean square	F-value	p-value	Status
Model	689.90	5	137.98	20.93	0.0001	Significant
A-Radius	369..66	1	369.66	56.07	＜0.0001	Significant
B-Voltage	280.51	1	280.51	42.55	0.0001	Significant
AB	10.49	1	10.49	1.59	0.2388	not Significant
A^2	6.84	1	6.84	1.04	0.3349	not Significant
B^2	22.39	1	22.39	3.40	0.0984	not Significant
Residual	59.33	9	6.59	-	-	-
Total	749.23	14	-	-	-	-
R^2	0.9208	-	-	-	-	-

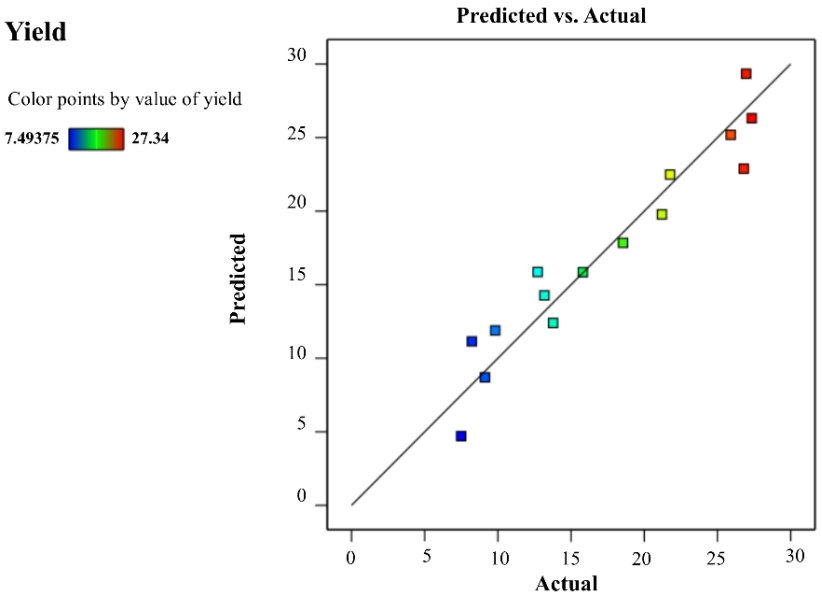

Figure 6: Predicted yields versus actual yields of electrospun PAN nanofibers

The relationship between the response and the factors can be visualized by the contour and three-dimensional response surface plots. Fig. 7 exhibited the contour and three-dimensional response surface plots of the yield of PAN nanofibers as a function of sphere radius and applied voltage. It was obvious that when the sphere radius remained constant, the yield of nanofibers increased with the increase of the voltage. And when the applied voltage kept constant, the yield of nanofibers increased first and then decreased with the increase of the sphere radius.

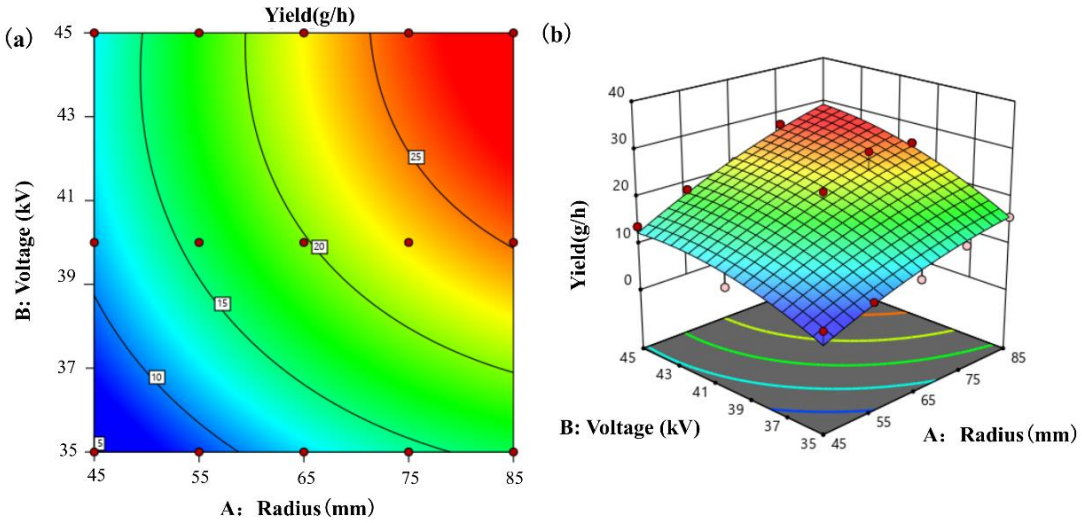

Figure 7: Contour (a) and three-dimensional (b) response surface plots of yield of PAN nanofiber as a function of sphere radius and applied voltage

3.4. Simulating electric field

In order to study the preparation mechanism of the SSFSE device, Maxwell 3D was used to simulate the electric field distributions in the SSFSE processes with solution reservoirs of different depths, as shown in Fig. 8. More uniform electric field distribution can help to produce finer and more uniform fiber [29]. Fig. 8 (a-1, b-1, c-1, d-1, e-1) represented the scalar plots of two-dimensional center section of the 3D electric field simulations in these SSFSE processes and the according local magnified view of the reservoir top edge. It could be seen that the maximum electric field intensities all distributed at the top edge of the copper reservoir, making it easier to produce jets. Fig.8 (a-3, b-3, c-3, d-3, e-3) showed the vector plots of the corresponding electric field simulations in the same areas. It was found that the directions of the electric fields were oriented directly towards to the collector due to the cylindrical symmetry of the solution reservoir and the cancellation of the vertical field components, causing the jets to be subjected to the upward electric field force. Fig. 8 (a-2, b-2, c-2, d-2, e-2) and Fig. 8 (a-4, b-4, c-4, d-4, e-4) exhibited the electric field distributions in the axial (0-180mm) direction and radial (0-100mm) direction on the upper surface center of the five SSFSE reservoirs, respectively. It illustrated that the electric field intensities in the axial direction decreased as the distance from the solution surface increased, and the electric field intensities in the radial direction first increased sharply, reached the maximum value at the top edge of the reservoir because of the electron transition from the solution to the copper, and then dropped sharply due to the electron transition from the copper to the air.

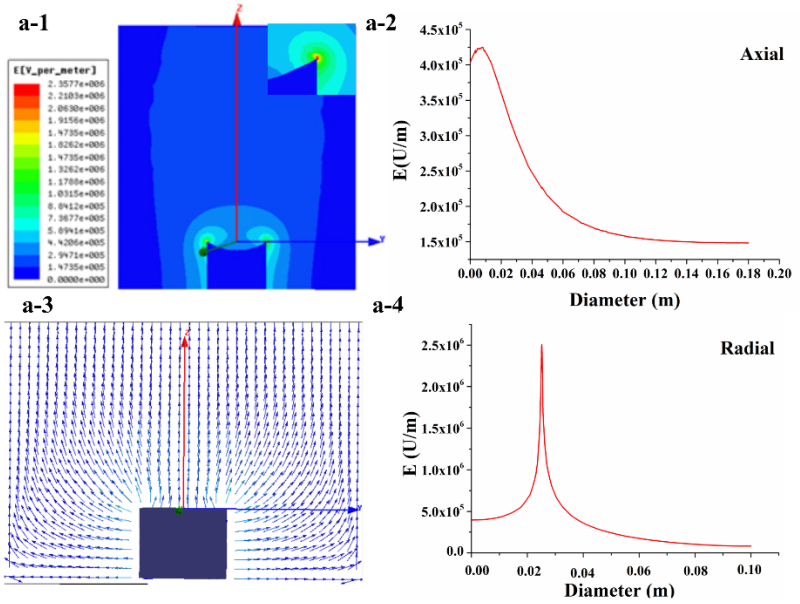

(a) SSFSE solution reservoir with a maximum depth of 7.58 mm

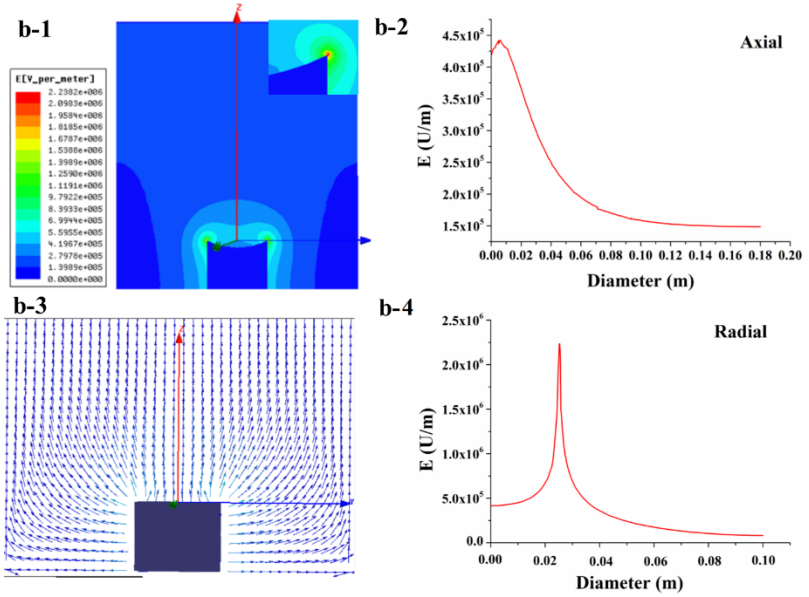

(b) SSFSE solution reservoir with a maximum depth of 6.01 mm

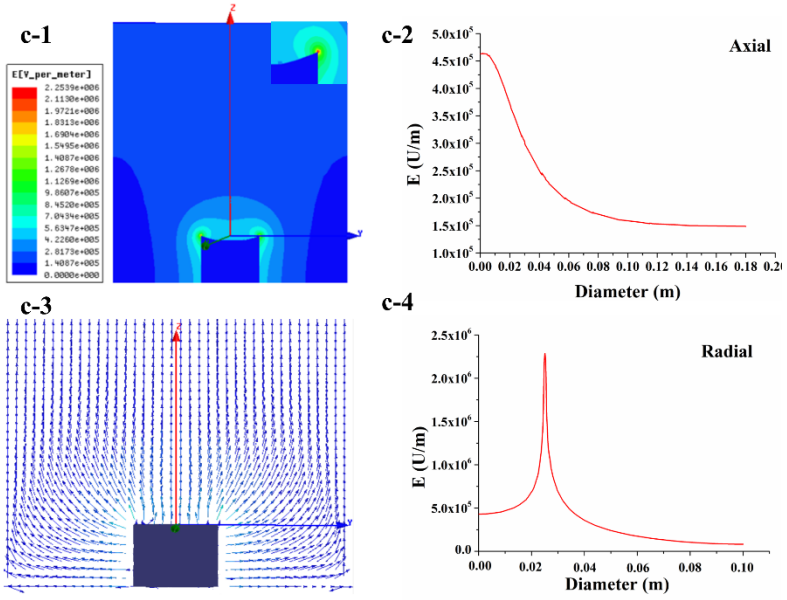

(c) SSFSE solution reservoir with a maximum depth of 5 mm

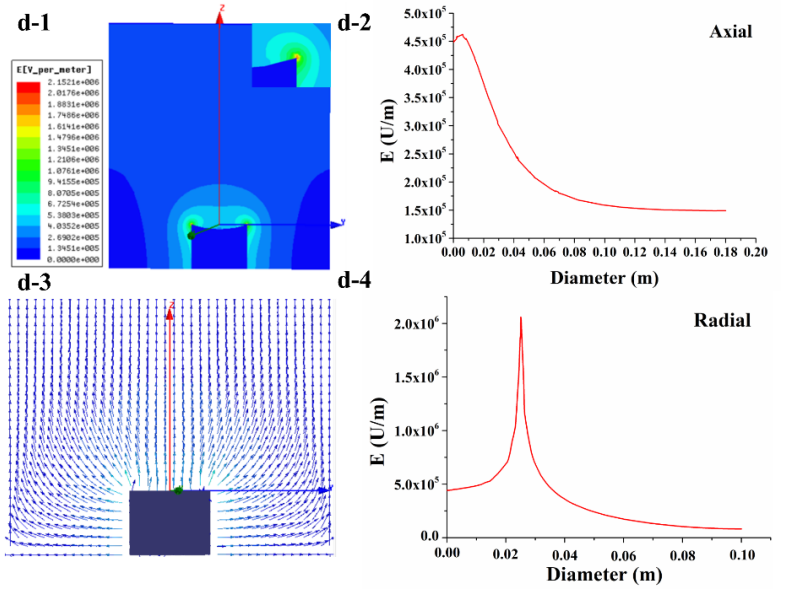

(d) SSFSE solution reservoir with a maximum depth of 4.29 mm

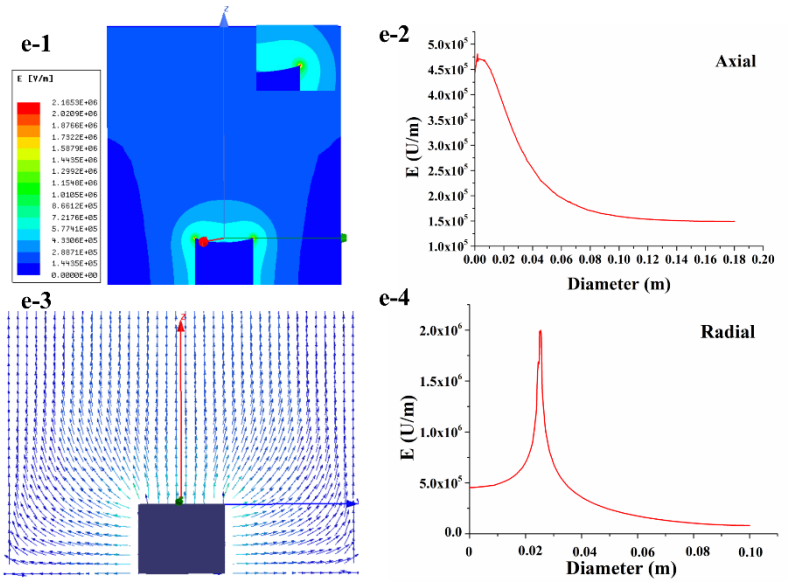

(e) SSFSE solution reservoir with a maximum depth of 3.76 mm

Figure 8: Simulation of the electric field distributions in five SSFSE devices with solution reservoirs of different depths at 40kV

To further compare the uniformity of electric field distributions of these five SSFSE processes, a parameter f is introduced, which is calculated by the following formula [25]. The smaller its value, the more uniform the electric field distribution [25].

$$f = \frac{E_{\max}}{E_{\mathrm{av}}} \tag{4}$$

where $E_{\max}$ is the maximum electric field intensity and E_{av} is the average electric field intensity.

The calculated values of $E_{\max}$, E_{av} and f in the radial (0-20 mm more than the corresponding radius) and axial (0-180 mm) directions of these five SSFSE processes were displayed in Table 5, respectively. It could be seen that as the solution reservoir depth decreased the values of $E_{\max}$ and f in the radial directions all decreased, but the values of E_{av} in the radial directions as well as the values of $E_{\max}$, E_{av} and f in the axial directions all increased. When the maximum depth of the solution reservoir was 7.58 mm, the values of $E_{\max}$, E_{av} and f in the axial direction as well as E_{av} in the radial direction were all minimum because of the deepest reservoir depth, but the values of $E_{\max}$ and f in the radial direction were maximum due to the tip discharge generated by the sharpest top edge of the reservoir, leading to the most non-uniform electric field distribution and relatively few jets produced, as indicated in Fig.3 (a). When the maximum depth of the solution reservoir was 4.29 mm, the values of f in the axial and radial directions were relatively smaller and the value of E_{av} was higher, which demonstrated the electric field distribution was more uniform and the electric field intensities were higher, leading to lots of uniform and stable jets produced from the solution surface, as exhibited in Fig. 3 (d), as well as the nanofibers obtained with highest quality and yield, as shown in Fig. 5 (d) and Fig. 4. When the maximum depth of the solution reservoir was 3.76 mm, due to the smallest reservoir depth, the values of $E_{\max}$, E_{av} and f in the axial direction as well as E_{av} in the radial direction were all maximum, but the values of $E_{\max}$ and f in the radial direction were minimum, which meant the electric field had the highest average intensity and the most uniform distribution. This led to the formation of unstable and outward expanding jets as well as too fast spinning speed, as illustrated in Fig.3 (e), which made it difficult for nanofibers to be fully stretched and collected, resulting in the nanofibers prepared with the largest diameter and lower yield, as indicated in Fig. 5 (e) and Fig. 4. The analysis

results of the electric field distributions were consistent with the experimental results, as shown in Fig.3, Fig. 4 and Fig. 5.

Table 5 The calculated values of E_{max}, E_{av} and f on the radial (0-20mm more than the corresponding radius) and the axial (0-180mm) directions of these five SSFSE processes.

h	E_{max} (V/m)		E_{av} (V/m)		f	
(mm)	Radial	Axial	Radial	Axial	Radial	Axial
7.58	2.51×10^6	4.25×10^5	5.86×10^5	2.07×10^5	4.28	2.05
6.01	2.28×10^6	4.43×10^5	5.97×10^5	2.10×10^5	3.77	2.11
5	2.24×10^6	4.64×10^5	6.04×10^5	2.12×10^5	3.75	2.19
4.29	2.06×10^6	4.62×10^5	6.08×10^5	2.13×10^5	3.39	2.17
3.76	2.00×10^6	4.81×10^5	6.12×10^5	2.14×10^5	3.27	2.25

4. Conclusion

In this paper, the effects of the solution reservoir depth on the SSFSE process as well as the quality and yield of PAN nanofibers were investigated experimentally and analyzed theoretically. The SSFSE process was observed by a high-speed camera, the morphology and the yield of PAN nanofibers obtained using the SSFSE were determined by a scanning electron microscopy (SEM) and a precise electronic balance, respectively. According to the experimental data, a RSM model was established to optimize the SSFSE process and evaluate the effect of the solution reservoir depth and the applied voltage on the yield of nanofibers. The values predicted by RSM indicated that the solution reservoir depth and the applied voltage all had great influences on the yield of nanofibers, which were consistent with the experimental results. Furthermore, the numerical simulation of the electric field distribution by Maxwell 3D in the SSFSE process demonstrated the preparation mechanism of SSFSE, which illustrated that PAN nanofibers with the highest quality and yield could be obtained by the SSFSE device using a solution reservoir with a maximum depth of 4.29 mm due to its higher average electric field intensity and more uniform electric field distribution. The simulation results were verified by experimental data.

Acknowledgments

The work is supported financially by National Natural Science Foundation of China (Grant No. 11672198), Jiangsu Higher Education Institutions of China (Grant No. 20KJA130001), Six Talent Peaks Project of Jiangsu Province (Grant No.GDZB-050), Science and Technology Guiding Project of China National Textile and Apparel Council (2020013), and PAPD (A Project Funded by the Priority Academic Program Development of Jiangsu Higher Education Institutions).

References

1. Huerta, R. R.; Silva, E. K.; El-Bialy, T. Saldaña M. D. A.; Ultrason Sonochem. 2019.
2. Kang, J.; Hwang, J. Y.; Huh, M.; Yun, S. I. Macromol. Res. 2020.

3. Avci, H.; Akkulak, E.; Gergeroglu, H.; Ghorbanpoor, H.; Uysal, O.; Sariboyaci, A.E.; Demir, B.; Soykan, M. N.; Pat, S.; Mohammadigharehbagh, R.; Ozel, C.; Cabuk, A.; Guzel, F. D. J Appl. Polym. Sci. 2020, 137.
4. Yin, J.; Xu, L. Int. J. Biol. Macromol. 2020, 160, 352-363.
5. Liu, H.; Zuo, B. Appl. Sci. 2018, 8, 296.
6. Shao, P.; Niu, B.; Chen, H.; Sun, P. Int. J. Biol. Macromol. 2018, 107, 1908-1914
7. Wu, Y.; Kelly, S. H.; Sanchez-Perez, L.; Sampson, J.; Collier, J. H. Biomater. Sci. 2020, 8(12).
8. Cheng, T.; Li, S.; Xu, L. Ahmed, A. Mater. Des. 2019, 178.
9. Wang, Y.; Cheng, T.; Xu, L. The J. Text, Inst, 2019, 110(12), 760-1766.
10. Wang, Y.; Song, Y.H.; Ye, C.W.; Xu, L. Beilstein J. Nanotechnol. 2020, 11, 1280-1290.
11. Liu, H. Y.; Xu, L.; Tang, X. P.; Si, N. Adv. Mater. Res. 2014, 905: 19-22.
12. Wei, L.; Yu, H. N.; Sun, R. J.; Liu, C. K.; Chen, M. Y.; Liu, H. J.; Xiong, J.; Qin, X. H. J. Ind. Text. 2020, 0(0), 1-14.
13. Zhou, Y.; Wang, H.; He, J.; Qi, K.; Ding, B.; Cui, S. J. Mater. Sci. 2018, 53(22), 15735-15745.
14. Liu, Y.; Guo, L. J. Nanosci. Nanotechnol. 2013, 13(2), 843-847.
15. Theron, S.A.; Yarin, A.L.; Zussman, E.; Kroll, E. Polymer. 2005, 46, 2889-2899.
16. Liu, S.L.; Huang, Y.Y.; Zhang, H.D.; Sun, B.; Zhang, J.C.; Long, Y.Z. Mater. Res. Innovations. 2014, 18, 833-837.
17. Jiang, G.; Johnson, L.; Xie, S. Open. Phys. 2019, 17, 313-319.
18. Jun-Jye, N.; Pitt, S. J. Polym. Res. 2018, 25(7): 155.
19. Tan, H. L.; Putrim M. K. S.; Idris, S. S.; Hartikainen, N.; Abu Bakar, N. F.; Keirouz, A.; Radacsi, N. J. Appl. Polym. Sci. 2020.
20. He, J.H.; Liu, Y.; Xu, L. Mater. Sci. Technol. 2010, 26, 1275-1287.
21. Forward, K. M.; Rutledge, G. C.; Free surface electrospinning from a wire electrode. Chem. Eng. J. 2012, 183, 492-503.
22. Shao, Z., Yu, L., Xu, L., Wang, M.: Nanoscale. Res. Lett. 2017, 12(1), 470.
23. Yu, L., Shao, Z., Xu, L., Wang, M.: Polymers. 2017, 9(12), 658.
24. Fang, Y., Xu, L., Wang, M.: Nanomaterials. 2018, 8(7), 471.
25. Fang, Y., Xu, L.: Beilstein J. Nanotechnol. 2019, 10, 2261-2274.
26. Ahmed, A., Yin, J., Xu, L., Khan, F.: J. Mater. Res. Technol. 2020, 9(4), 9059-9072.
27. Banikazemi, S.; Rezaei, M.; Rezaei, P.; Babaie, A.; Alireza Eyvazzadehalajahi, A. Polym. Adv. Technol. 2020, 31(10), 2199-2208.
28. Xie, S.; Zeng, Y. Effects of electric field on multineedle electrospinning: Experiment and simulation study. Ind. Eng. Chem. Res. 2012, 51, 5336-5345.
29. Ipakchi, H.; Masoud Rezadoust, A.; Esfandeh, M.; Mirshekar, H. J. Compos. Mater. 2020, 54, 363-378.